Molecular-beam optical Stark and Zeeman study of the $A\,^2\Pi$–$X\,^2\Sigma^+$ (0,0) band system of BaF

Timothy C. Steimle,* Sarah Frey, and Anh Le
Department of Chemistry and Biochemistry, Arizona State University, Tempe, Arizona 85287-1604, USA

David DeMille and David. A. Rahmlow†
Department of Physics, Yale University, P.O. Box 208120, New Haven, Connecticut 06520, USA

Colan Linton
Centre for Laser Atomic and Molecular Sciences, Physics Department, University of New Brunswick, P.O. Box 4400, Fredericton, New Brunswick, Canada E3B 5A3

(Received 18 April 2011; published 19 July 2011)

The $A\,^2\Pi - X\,^2\Sigma^+$ (0,0) band system of barium monofluoride (BaF) has been recorded using high-resolution laser-induced fluorescence spectroscopy both field-free and in the presence of static magnetic and electric fields. The field-free spectra for the ^{135}BaF, ^{137}BaF, and ^{138}BaF isotopologues were modeled to generate an improved set of spectroscopic constants for the $A\,^2\Pi(\upsilon=0)$ and $X\,^2\Sigma^+(\upsilon=0)$ states. The observed optical Stark shifts for the ^{138}BaF isotopologue were analyzed to produce the permanent electric dipole moments of 1.50(2) and 1.31(2) D for the $A\,^2\Pi_{1/2}(\upsilon=0)$ and $A\,^2\Pi_{3/2}$ $(\upsilon=0)$ states, respectively. The observed optical Zeeman shifts for the ^{138}BaF isotopologue were analyzed to produce a set of magnetic g factors for the $A\,^2\Pi(\upsilon=0)$ and $X\,^2\Sigma^+(\upsilon=0)$ states.

DOI: 10.1103/PhysRevA.84.012508 PACS number(s): 33.20.Kf

I. INTRODUCTION

There is renewed interest in measuring and predicting the properties of barium monofluoride, BaF, because of its use as a sensitive experimental venue for quantification of P- and P,T-odd effects [1–9]. The determination of the electric dipole moment (EDM) of the electron, d_e, provides insight into the violation of parity inversion symmetry (P) and time-reversal invariance (T). Such effects are nuclear spin independent and studies of both the even and odd BaF isotopologues are relevant. The interaction of the nuclear anapole moment, a P-odd magnetic moment induced by weak interactions within the nucleus, with the spin of the penetrating electrons is a nuclear spin dependent parity violation effect. This latter interaction can be probed via studies of only the odd BaF isotopologues. The effective Hamiltonian operator for the $X\,^2\Sigma^+$ electronic state of BaF, including the parity non-conservation (PNC) relevant terms, is [1,9]:

$$\begin{aligned} H^{\text{eff}}(^2\Sigma) = {} & B\mathbf{N}^2 + \gamma\mathbf{N}\cdot\mathbf{S} + b_F\mathbf{I}\cdot\mathbf{S} \\ & + c\left(I_z S_z - \frac{1}{3}\mathbf{I}\cdot\mathbf{S}\right) + eq_0Q\frac{3I_z - I^2}{4I(2I-1)} \\ & + W_A k_A \mathbf{n}\times\mathbf{I}\cdot\mathbf{S} + (W_S k_S + W_d d_e)\mathbf{S}\cdot\mathbf{n}, \end{aligned} \quad (1)$$

where $\mathbf{N}$ is the angular momentum operator excluding electronic spin $\mathbf{S}$ and nuclear spin $\mathbf{I}$, and $\mathbf{n}$ is a unit vector along the bond. The first five terms in (1) are commonly used to model the fine (via the B and γ terms), Fermi contact, and dipolar magnetic hyperfine (via the b_F and c terms), and the electric quadrupole hyperfine (via the eq_0Q term) interactions. The sixth term describes the interaction of the anapole moment of the nucleus k_A, with the electron spin, the seventh a scalar electron-nucleus interaction, and the last the interaction of d_e with the effective electric field, W_d. Determination of the ^{135}BaF and ^{137}BaF hyperfine parameters is particularly relevant to parity violation studies, because these parameters are the most sensitive probes of the electronic wave function in the region of the Ba nucleus. In parity nonconservation studies the constants W_A, W_S, and W_d of (1) are calculated as expectation values of appropriate symmetry-violating operators over the electronic wave function in the region of the Ba nucleus. Thus, a comparison of experimentally measured hyperfine constants, which also depend upon the electronic wave function in the region of the Ba nucleus, is the most rigorous gauge of the reliability of the predicted W_A, W_S , and W_d values.

Experimental schemes for measuring P- and P,T-odd effects in BaF exploit laser-induced fluorescence detection using the $A\,^2\Pi$–$X\,^2\Sigma^+$ (0,0) band system. In addition, the study of P-odd effects relies on Zeeman tuning of opposite-parity levels to near degeneracy in a large magnetic field, and on mixing of these levels due to an applied electric field. Consequently, a spectroscopic understanding of the energy levels of both the $A\,^2\Pi(v=0)$ and $X\,^2\Sigma^+$ $(v=0)$ states, as well as Stark and Zeeman effects in these states, is required. Here we report on the analysis of the $A\,^2\Pi$–$X\,^2\Sigma^+$ (0,0) band system recorded at near the natural linewidth limit [full width at half maximum (FWHM) ≈30 MHz]. Spectra were recorded field-free and in the presence of static electric and magnetic fields. An improved set of fine and hyperfine parameters for the $A\,^2\Pi(\upsilon=0)$ state is determined for the

*Tsteimle@asu.edu
†Current Address: Department of Physics, University of Connecticut, 2152 Hillside Road, U-3046 Storrs, CT 06269-3046.

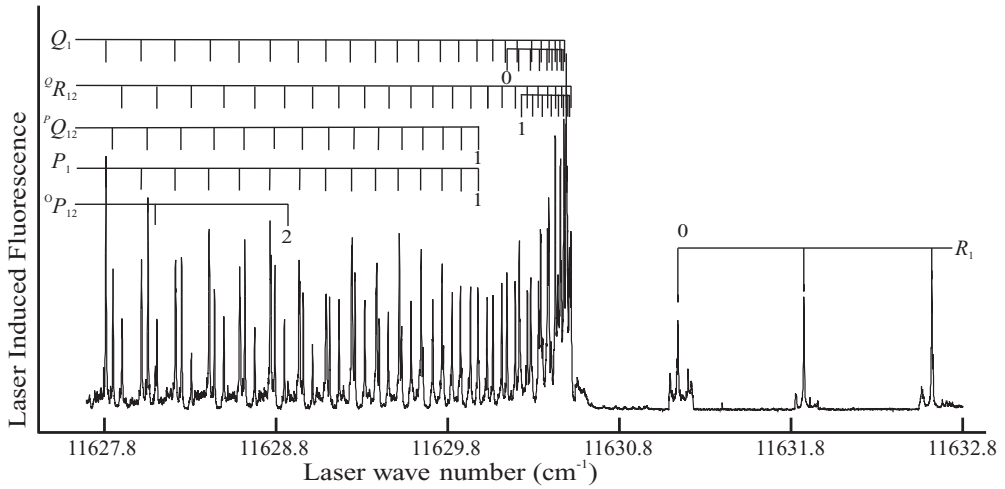

FIG. 1. Field-free spectrum of $A\,^2\Pi_{1/2}$–$X\,^2\Sigma^+(0,0)$ subband system of BaF.

^{135}BaF, ^{137}BaF, and ^{138}BaF isotopologues. The permanent electric dipole moment μ_e for the $A\,^2\Pi_{1/2}(\upsilon=0)$ and $A\,^2\Pi_{3/2}$ $(\upsilon=0)$ states and the magnetic g factors for the $A\,^2\Pi(\upsilon=0)$ and $X\,^2\Sigma^+(\upsilon=0)$ states of ^{138}BaF were determined from an analysis of the observed Stark and Zeeman shifts, respectively.

The field-free energies of the $X\,^2\Sigma^+(\upsilon=0)$ state of the ^{138}BaF and ^{137}BaF isotopologues are well characterized. The pure rotational spectra of ^{138}BaF [10] and ^{137}BaF [11] have been recorded and analyzed to produce a set of fine and hyperfine constants for the $X\,^2\Sigma^+(\upsilon=0)$ state. An improved set of ^{19}F magnetic hyperfine constants for the ^{138}BaF isotopologue was obtained from the analysis of the microwave-optical double resonance (MODR) spectrum [12]. In the same study, the electric field induced shifts of the rotational levels of the $X\,^2\Sigma^+(\upsilon=0)$ state were measured from which a μ_e of 3.170(3) D was determined. There have been no reported experimental measurements of μ_e for the $A\,^2\Pi$ state. The $X\,^2\Sigma^+(\upsilon=0)$ state has also been studied by high-resolution Fourier transform infrared emission spectroscopy [13]. In that study, numerous vibration-rotation bands were analyzed for the three most abundant isotopologues from which Dunham coefficients were derived.

The $A\,^2\Pi$ state is less well characterized. The $A\,^2\Pi-X\,^2\Sigma^+$ (0,0) band system of the main isotopologue,^{138}BaF, has been previously characterized from analysis of the near Doppler limited resolution Fourier transform spectra of the thermal emission and the Ar^+ and Kr^+ ion laser-induced fluorescence [14–16]. It was observed that the $A\,^2\Pi$ state was perturbed by the nearby $A'^2\Delta$ and $B^2\Sigma^+$ states. Effective molecular constants were obtained by treating the trio of states as a d complex. The radiative lifetime of the $A\,^2\Pi_{1/2}(\upsilon=0)$ [17] and $A\,^2\Pi_{3/2}(\upsilon=0)$ [18] states were measured to be 46.1 and 56.0 ns, respectively.

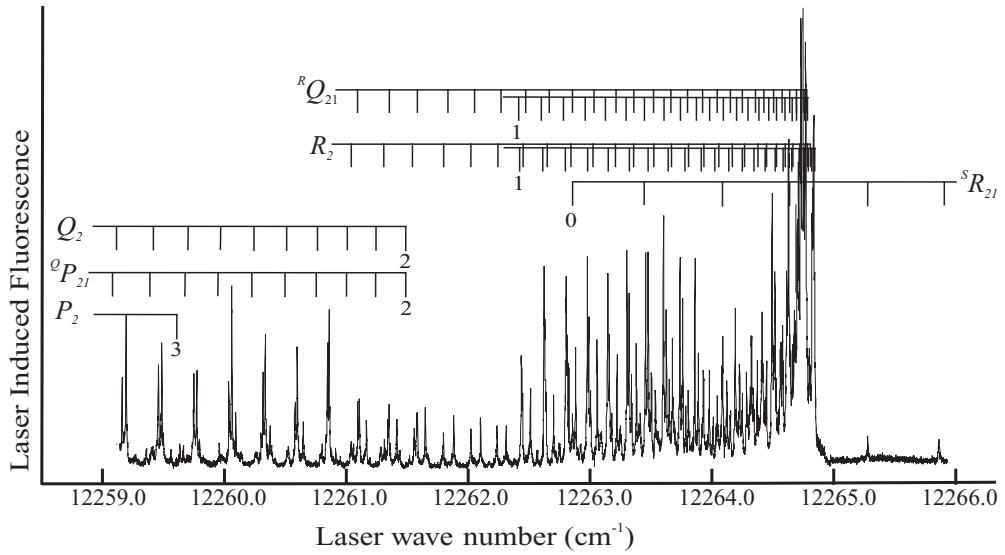

FIG. 2. Field-free spectrum of $A\,^2\Pi_{3/2}$–$X\,^2\Sigma^+(0,0)$ subband system of BaF.

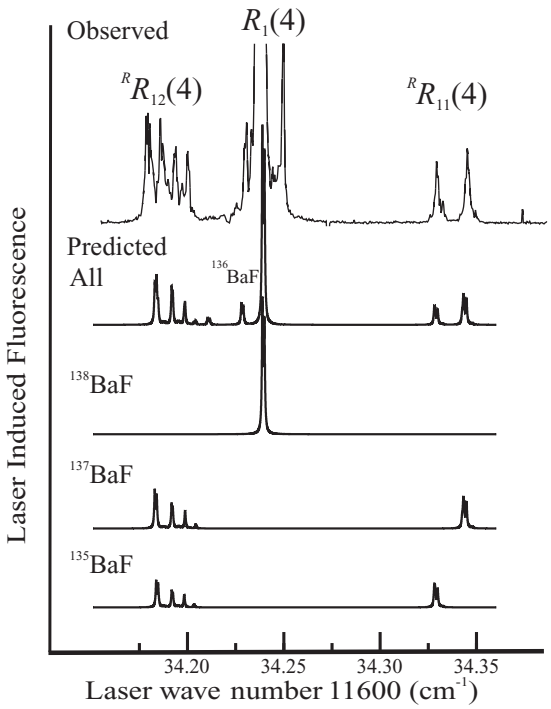

FIG. 3. Observed and predicted spectra of the $A\,^2\Pi_{1/2}$–$X\,^2\Sigma^+(0,0)$ subband system of BaF in the region of the $R_1(4)$ line ($\nu =$ 11634.25 cm^{-1}) of the ^{138}BaF isotopologue. The predicted spectra were obtained using the optimized parameters of Table III and a linewidth of 20 MHz.

There are no high-level *ab initio* predictions for the $X\,^2\Sigma^+$ and $A\,^2\Pi$ states. A semi-empirical electrostatic polarization model developed by Törring *et al.* [19] predicts that $\mu_e = 3.47$ and 4.95 D for the $X\,^2\Sigma^+$ and $A\,^2\Pi$ states, respectively. A similar model developed by Mestdagh and Visticot [20] predicts nearly identical values. A ligand field theory (LFT) [21] predicts $\mu_e = 3.89$ and 3.45 D for the $X\,^2\Sigma^+$ and $A\,^2\Pi$ states, respectively.

II. EXPERIMENT

The supersonic molecular beam production and laser-induced fluorescent detection schemes are similar to those used in the previous measurements of SrF [22] and YbF [23,24]. A continuously rotating barium metal rod was ablated in a supersonic expansion of approximately 5% sulfur hexafluoride (SF_6) seeded in an argon carrier gas with a backing pressure of approximately 3 MPa. The pulsed free-jet expansion was skimmed to form a well-collimated molecular beam which was crossed with a single longitudinal mode, continuous wave, Ti:sapphire laser approximately 50 cm downstream from the source. The laser power was attenuated to approximately 20 mW and lightly focused (focal length = 1 m) to avoid power broadening. Spectral line widths of less than 40 MHz FWHM were observed.

The absolute wave numbers were determined to an accuracy of ± 0.003 cm^{-1} by simultaneously recording the Doppler limited I_2 absorption spectrum [25,26]. Interpolation between I_2 absorption features was achieved by simultaneously recording the transmission of two confocal étalons. One étalon was actively stabilized and calibrated to have a free spectral range of 749.14 MHz. A second, unstabilized étalon with a free spectral range of 75.7 MHz was used to interpolate between transmission peaks of the stabilized étalon.

The optical Zeeman spectrometer [27] and optical Stark spectrometer [28] have been described previously. A 0–1.0 kG, homogeneous magnetic field was generated using a homemade electromagnet in the interaction region of the molecular beam and laser. The magnetic field was measure using a commercial Gauss meter. Static electric field strengths of up to 2000 V/cm were generated by application of a voltage across a pair of conducting plates straddling the region of molecular fluorescence. The electric field was measure by combination of a commercial volt meter and mechanical measurement of the plate separation. A polarization rotator and polarizing filter were used to orient the static electric or magnetic field vector of the linearly polarized laser radiation either parallel "$\parallel$" or perpendicular "$\perp$" to that of the applied field resulting in $\Delta M_F = 0$ or $\Delta M_F = \pm 1$ selection rules. The combined systematic error associated with the measurement of the magnetic and electric field induced frequency shifts and the field strength is estimated to be less than 2%.

III. OBSERVATION

A. Field-free Spectra

Portions of the field-free excitation spectrum in the region of the $A\,^2\Pi_{1/2}$–$X\,^2\Sigma^+$ (0,0) and $A\,^2\Pi_{3/2}$–$X\,^2\Sigma^+(0,0)$ subbands are presented in Figs. 1 and 2, respectively. Enlarged portions of the field-free laser-induced fluorescence (LIF) spectra in

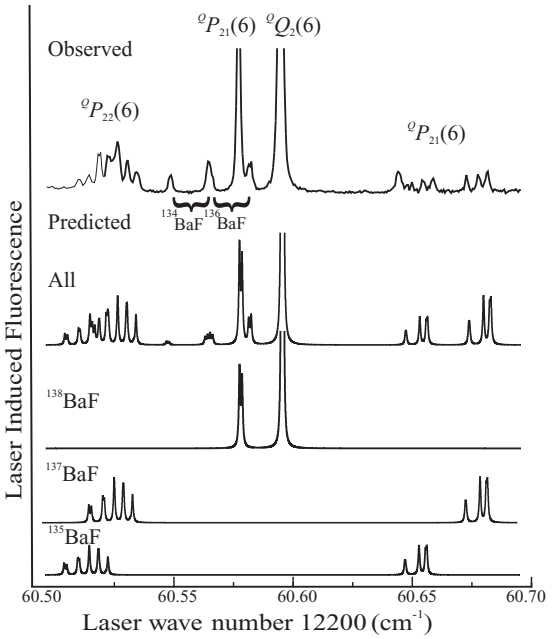

FIG. 4. Observed and predicted spectra of the $A\,^2\Pi_{3/2}$–$X\,^2\Sigma^+(0,0)$ subband system of BaF in the region of the $Q_2(6)$ line ($\nu = 12260.60$ cm^{-1}) and $^{Q}P_{21}(6)$ line ($\nu = 12260.58$ cm^{-1}) of the ^{138}BaF isotopologue. The predicted spectra were obtained using the optimized parameters of Table III and a linewidth of 20 MHz.

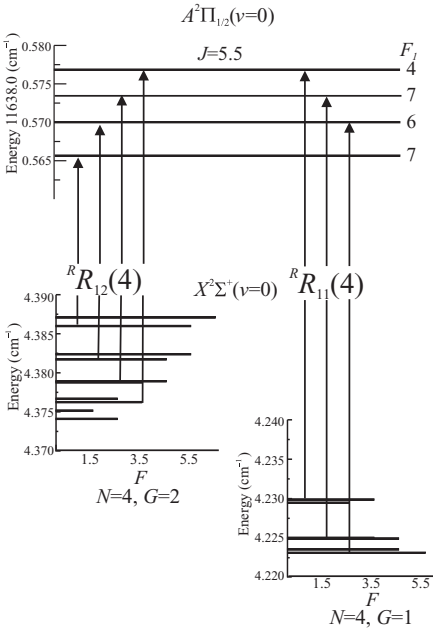

FIG. 5. Predicted energy level pattern associated with the $^RR_{12}(4)$ line (ν = 11634.19 cm^{-1}) and the $^RR_{11}(4)$ line (ν = 11634.35 cm^{-1}) of the ^{137}BaF isotopologue. The assignments of the spectral features of Fig. 3 are indicated. The energies were calculated using the optimized parameters of Table III.

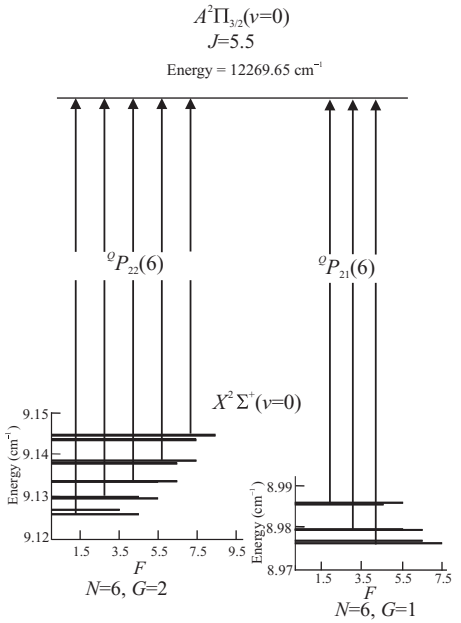

FIG. 6. Predicted energy level pattern associated with the $^QP_{22}(6)$ line (ν = 12260.52 cm^{-1}) and the $^QP_{21}(6)$ line (ν = 12260.68 cm^{-1}) of the ^{137}BaF isotopologue. The assignments of the spectral features of Fig. 4 are indicated. The energies were calculated using the optimized parameters of Table III.

the regions of the $R_1(4)$ ($\nu = 11634.25$ cm^{-1}) and $^QQ_2(6)$ ($\nu = 12260.60$ cm^{-1}) lines are presented in Figs. 3 and 4, respectively. The relative positions of the lines associated with the various isotopologues are evident in Figs. 3 and 4. The spectra are congested in part because there are seven naturally occurring isotopes of barium: ^{130}Ba(0.11%), ^{132}Ba(0.10%), ^{134}Ba(2.42%), ^{135}Ba(6.59%), ^{136}Ba(7.85%), ^{137}Ba(11.23%), and ^{138}Ba(71.70%). Transitions associated with the ^{135}BaF, ^{136}BaF, ^{137}BaF, and ^{138}BaF isotopologues are readily identified in Figs. 1–3. Spectral lines of the odd isotopologues exhibit a large splitting due to a Ba-hyperfine interaction in the $X\,^2\Sigma^+(\upsilon = 0)$ state. The nuclear magnetic g factors for ^{135}Ba($\mathbf{I} = 3/2$) and ^{137}Ba($\mathbf{I} = 3/2$) are $+0.5586$ and $+0.6249$, respectively, and the quadrupole moments are $+18$ and $+28$ fm^2, respectively. The ^{19}F($\mathbf{I} = 1/2$) magnetic hyperfine splitting is much smaller because the unpaired electron in the $A\,^2\Pi$ and $X\,^2\Sigma^+$ states is centered on the metal nucleus. The predicted energy levels associated with lines of the ^{137}BaF isotopologue in the region of the $^RR_{11}(4)$ and $^QQ_2(6)$ lines of the ^{138}BaF isotopologue, obtained using the finalized optimized parameters, are presented in Figs. 5 and 6, respectively, and illustrates the relative hyperfine splitting.

The energy level patterns for the low-rotational levels of the $X\,^2\Sigma^+$ state of the even barium isotopologues are those of a molecule near the Hund's case ($b_{\beta\mathrm{J}}$) limit with the approximately good intermediate quantum number J resulting from coupling the rotational angular momentum $\mathbf{N}$ with the electron spin angular momentum $\mathbf{S}$. Each rotational level of a given J of the even isotopologues splits into two levels designated by the total angular momentum F due to the ^{19}F($\mathbf{I} = 1/2$) magnetic hyperfine splitting. The resulting Hund's case ($b_{\beta\mathrm{J}}$) vector coupling appropriate for even barium isotopologues can be written as

$$\mathbf{S} + \mathbf{N} = \mathbf{J}, \qquad \mathbf{I}_1(^{19}\mathrm{F}) + \mathbf{J} = \mathbf{F}, \tag{2}$$

which corresponds to the basis set $|\eta\Lambda\rangle|(SN)J(J\,I_1)F\,\rangle$.

The large ^{137,135}Ba magnetic hyperfine interaction in the $X\,^2\Sigma^+$ state causes the energy level pattern for the low-rotational levels of the odd isotopologues to be those

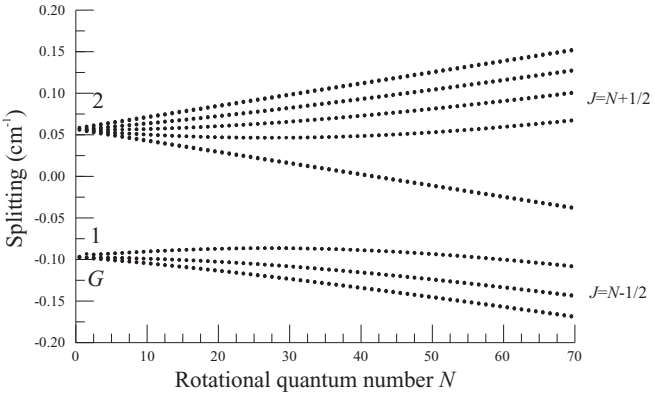

FIG. 7. ^{137}BaF isotopologue spin-rotation and hyperfine energy level pattern for the $X\,^2\Sigma^+$ ($\nu = 0$) state as a function of rotational quantum number N. The low rotational levels are those of a Hund's case ($b_{\beta S}$) molecule with G being the appropriate intermediate quantum number, and those of the high rotational levels a Hund's case ($b_{\beta J}$) molecule where J is the appropriate intermediate quantum number.

of a molecule near the Hund's case ($b_{\beta S}$) limit. The approximately good intermediate quantum number G ($=1$ and 2) results from coupling the ^{137,135}Ba nuclear spin angular momentum $\mathbf{I_1}$ with the total electron spin angular momentum $\mathbf{S}$. The ^{19}F nuclear spin is weakly coupled to $\mathbf{G}$ to produce the total angular momentum $\mathbf{F}$. The Hund's case ($b_{\beta S}$) vector coupling for low rotational levels can be written as

$$\mathbf{S}+\mathbf{I}_1(^{137,135}\mathrm{Ba})=\mathbf{G}(^{137,135}\mathrm{Ba}),\quad \mathbf{N}+\mathbf{G}(^{137,135}\mathrm{Ba})=\mathbf{F}_1,$$
$$\mathbf{F}_1+\mathbf{I}_2(^{19}\mathrm{F})=\mathbf{F}, \tag{3}$$

which corresponds to the basis function $|\eta\Lambda\rangle|(SI_1)G(GN)F_1(F_1I_2)F\rangle$. The electron spin decouples from the nuclear spin with increasing rotation, and the energy level pattern of the $X\,^2\Sigma^+$ state of odd isotopologues gradually transforms to that of a molecule near the Hund's case ($b_{\beta J}$) limit. As an illustration, the energy level pattern of the $X\,^2\Sigma^+(v=0)$ state of ^{137}BaF as a function of rotation, predicted using the previously determined fine and hyperfine parameters [11], is illustrated in Fig. 7. The contribution due to rotation [$\approx B\times N(N+1)$] has been subtracted to emphasize the spin-rotation and hyperfine contributions.

The Ba hyperfine interactions are much smaller in the $A\,^2\Pi$ state, and the energy level patterns for the low-rotational levels of both the even and odd barium isotopologues are those of a molecule near the Hund's case ($a_{\beta J}$) limit with the electron spin quantized in the molecular frame and having a projection, Σ. A Hund's case ($a_{\beta J}$) coupling scheme, with the nuclear spin sequentially coupled, is appropriate for all the isotopologues:

$$\mathbf{J}+\mathbf{I}_1(^{135,137}\mathrm{Ba})=\mathbf{F}_1,\quad \mathbf{F}_1+\mathbf{I}_2(^{19}\mathrm{F})=\mathbf{F}. \tag{4}$$

The corresponding basis function is $|\eta\Lambda\rangle|S\Sigma\rangle|J\Omega(JI_1)F_1(F_1I_2)F\rangle$. The inclusion of $\mathbf{I}_2$ (^{19}F), even though the ^{19}F($I=1/2$) interaction is not fully resolved, facilitates spectral simulation.

A conventional $^2\Pi$ (case $a_{\beta J}$)–$^2\Sigma^+$ (case $b_{\beta J}$) labeling scheme of $^{\Delta N}\Delta J_{F_i' F_i''}(N'')$ [29], where F_i'' and F_i' subscripts designate the spin components of the $X\,^2\Sigma^+$ and $A\,^2\Pi$ states, respectively, is appropriate for the even isotopologues. In the cases where $\Delta N=\Delta J$ and $F_i''=F_i'$ it is customary to drop the superscript and the second subscript. The 12 branches of the $^2\Pi$ (case $a_{\beta J}$)–$^2\Sigma^+$ (case $b_{\beta J}$) labeling scheme (P_1, Q_1, R_1, $^PQ_{12}$, $^OP_{12}$, $^QR_{12}$, P_2, Q_2, R_2, $^RQ_{21}$, $^QP_{21}$, and $^SR_{21}$) are readily assigned (see Figs. 1– 4). The intermediate quantum number J is not appropriate for the low-rotational levels of the $X\,^2\Sigma^+$ state of the odd isotopologues and hence neither is the F_i'' subscript in the conventional $^2\Pi$ (case $a_{\beta J}$)–$^2\Sigma^+$ (case $b_{\beta J}$) branch designation. It is customary to replace F_i'' with the intermediate approximately good quantum number G'' of the Hund's case ($b_{\beta S}$) coupling scheme. The 12 branches of the $^2\Pi$ (case $a_{\beta J}$)–$^2\Sigma^+$ (case $b_{\beta J}$) labeling scheme regroup into 16 branch features of the $^2\Pi$ (case $a_{\beta J}$)–$^2\Sigma^+$ (case $b_{\beta S}$) scheme. The branches are designated as $^OP_{1G}$, $^PP_{1G}+{}^PQ_{1G}$, $^QQ_{1G}+{}^QR_{1G}$, and $^RR_{1G}$ for the $^2\Pi_{1/2}$ (case $a_{\beta J}$)–$^2\Sigma^+$ (case $b_{\beta S}$) subband and $^PP_{2G}$, $^QP_{2G}+{}^QQ_{2G}$, $^RQ_{2G}+{}^RR_{2G}$, and $^SR_{2G}$ for the $^2\Pi_{3/2}$ (case $a_{\beta J}$)–$^2\Sigma^+$ (case $b_{\beta S}$) subband with $G=1$ and 2. The abbreviations $^PP_{1G}$, $^QQ_{1G}$, $^QP_{2G}$, and $^RQ_{2G}$ for the $^PP_{1G}+{}^PQ_{1G}$, $^QQ_{1G}+{}^QR_{1G}$, $^QP_{2G}+{}^QQ_{2G}$, and $^RQ_{2G}+{}^RR_{2G}$ branches, respectively, are used in Figs. 3–6 and below.

A total of 439 transitions in the $A\,^2\Pi$–$X\,^2\Sigma^+$ (0,0) band were measured and assigned: 73, 99, and 267 for the ^{135}BaF, ^{137}BaF, and ^{138}BaF isotopologues, respectively. The observed and calculated transition wave numbers, based upon the final optimized parameters, and associated assignments for the ^{138}BaF,^{137}BaF, and^{135}BaF isotopologues are listed in Tables I, II, and III, respectively, of the Supplemental Tables [30].

B. Stark spectra

The $^SR_{21}(0)$ ($\nu=12262.88$ cm^{-1}) and $^OP_{12}(2)$ ($\nu=11628.96$ cm^{-1}) lines of the ^{138}BaF isotopologue were selected for optical Stark studies. The observed and predicted spectra for the $^SR_{21}(0)$ line recorded field-free and in the presence of a 899.4 V/cm static field with perpendicular orientation are presented in Fig. 8. The associated energy levels as a function of applied field are also presented. The field-free line rapidly splits into four components due to the near degeneracy of Λ doublets associated with the $J=3/2$ level of the $A\,^2\Pi_{3/2}$ state. The pattern of four features slightly shifts to higher wave numbers due to the second-order Stark tuning of the $N=0$ rotational level of the $X\,^2\Sigma^+$ state. The observed and predicted spectra for the $^OP_{12}(2)$ line recorded field-free and in the presence of a 2940 V/cm static field with parallel orientation are presented in Fig. 9. The associated energy levels as a function of applied field are also presented. The field-free spectral feature weakly tunes to lower wave number due primarily to the second-order Stark tuning in the e-parity component of the $J=1/2$ level of the $A\,^2\Pi_{1/2}$ state. The Λ doubling of the $J=1/2$ level (i.e., the separation between the e- and f-parity components) is 0.2589 cm^{-1} ($=p+2q$). A total of 17 Stark-induced shifts for the $^SR_{21}(0)$ line and 14 Stark-induced shifts for the $^OP_{12}(2)$ line were assigned and precisely measured. Measured shifts and the difference between the measured and predicted shifts are listed in Table I.

C. Zeeman spectra

The $R_1(0)$ ($\nu=11631.28$ cm^{-1}) and $^SR_{21}(0)$ ($\nu=12262.88$ cm^{-1}) lines of the ^{138}BaF isotopologue were selected for optical Zeeman studies. The $R_1(0)$ line recorded field-free and in the presence of 714 G parallel and 724 G perpendicular magnetic fields are presented in Fig. 10. The associated energy levels as a function of applied magnetic field, and the assignments, are also presented. The Zeeman tuning of the upper energy terminus of the $R_1(0)$ line (i.e., the "–" parity component of the $J=3/2$ rotational level in the $A\,^2\Pi_{1/2}$ spin-orbit substate) is small and would be nearly zero in the Hund's case (a) limit. The $^SR_{21}(0)$ line recorded field-free and in the presence of a 192 G perpendicular magnetic field is presented in Fig. 11. The associated energy levels as a function of applied magnetic field, and the assignments, are also presented. The

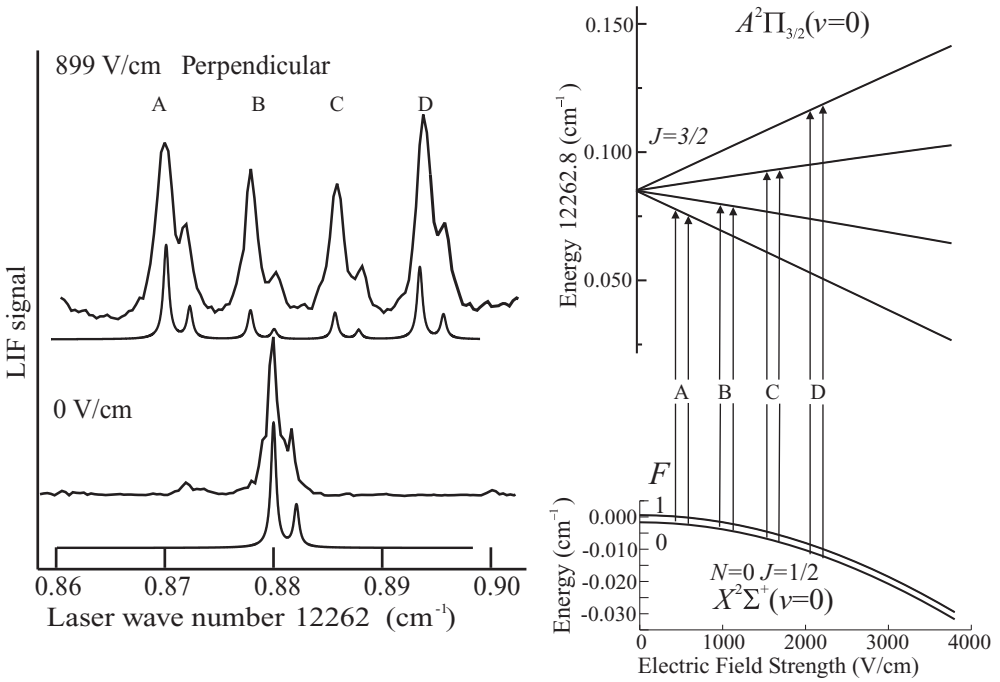

FIG. 8. Observed and predicted ${}^{S}R_{21}(0)$ line of the ^{138}BaF isotopologue recorded field-free and in the presence of a 899.4 V/cm static field with perpendicular orientation and the associated energy levels as a function of applied field. The near degeneracy of the Λ-doublets in the $J = 3/2$ level of the $A\,^2\Pi_{3/2}$ state results in a linear Stark tuning of the energy levels.

Zeeman tuning of the upper energy terminus of the ${}^{S}R_{21}(0)$ line (i.e., "–" parity component of the $J = 3/2$ rotational level in the $A\,^2\Pi_{3/2}$ spin-orbit component) is significant because the energy level pattern is near the Hund's case (a) limit. The measured 34 magnetically induced shifts of the ${}^{S}R_{21}(0)$ line and 42 shifts of the $R_1(0)$ line, along with the quantum number assignments, are presented in Table II. The differences between the observed shifts and those predicted using the optimized magnetic g factors (see below) are also given.

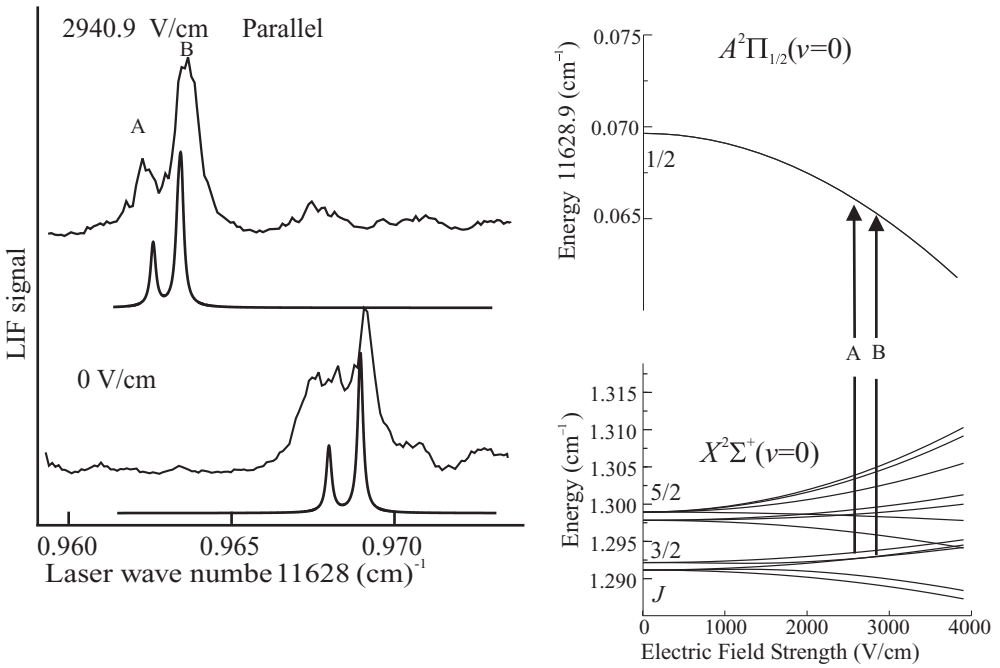

FIG. 9. Observed and predicted ${}^{O}P_{12}(2)$ line of the ^{138}BaF isotopologue recorded field-free and in the presence of a 2940.9 V/cm static field with parallel orientation and the associated energy levels as a function of applied field. The large Λ doubling ($= 0.257$ cm^{-1}) of the $J = 1/2$ levels of the $A\,^2\Pi_{1/2}$ state results in a second-order Stark effect.

TABLE I. Observed and calculated Stark shifts for the $A\,^2\Pi$–$X\,^2\Sigma^+(0,0)$ band system of ^{138}BaF.

Branch, pol	Field (V/cm)	Assign[a]	Shift (MHz)	Obs-Calc[b]
P_{12} (2), ∥	806	A	−25	−9
	1612	A	−64	−1
	1742	A	−79	−7
		B	−78	−8
	2014	A	−103	−7
		B	−89	3
	2342	A	−127	2
		B	−128	−2
	2416	A	−136	1
		B	−125	8
	2941	A	−207	−4
		B	−194	2
	3541	A	−292	4
		B	−281	2
	Std. dev. = 6 MHz			
$^SR_{21}(0)$, ⊥	601	D	259	−1
	601	C	93	−8
	601	B	−66	−10
	601	A	−223	−9
	899	D	412	6
	899	C	173	3
	899	B	−70	−3
	899	A	−307	−5
	1202	D	549	−17
	1202	C	239	−10
	1202	B	−376	6
	1501	B	−67	−11
	1501	A	−439	10
	1742	D	887	7
	1742	C	416	−4
	1742	B	−47	−8
	1742	A	−500	−5
	Std. dev. = 8 MHz			

[a]Refers to transitions indicated in Figs. 6 and 7.

[b]Calculated shifts obtained using optimized μ_e of 1.50(2) and 1.31(2) D for the $A\,^2\Pi_{1/2}(v=0)$ and $A\,^2\Pi_{3/2}(v=0)$ states and previously determined μ_e of 3.170(3) D for the $X\,^2\Sigma^+(v=0)$ state [12].

IV. ANALYSIS

A. Field free

The observed transition wave numbers of the molecular beam optical spectrum were directly fit to an effective Hamiltonian for the $X\,^2\Sigma^+$ $(v=0)$ and $A\,^2\Pi$ $(v=0)$ state. The effective Hamiltonian for the $X\,^2\Sigma^+$ $(v=0)$ state for the ^{138}BaF isotopologue was taken as

$$\mathbf{H}^{\text{eff}}(^2\Sigma^+) = B\mathbf{N}^2 - D\mathbf{N}^4 + \gamma\mathbf{N}\cdot\mathbf{S} + b_F(^{19}\text{F})\mathbf{I}\cdot\mathbf{S} + c(^{19}\text{F})\left(I_zS_z - \frac{1}{3}\mathbf{I}\cdot\mathbf{S}\right), \quad (5)$$

where **N** is the angular momentum operator excluding electronic and nuclear spins, **S** and **I**, respectively. The effective Hamiltonian for the $X\,^2\Sigma^+$ $(v=0)$ state for the ^{135}BaF and ^{137}BaF isotopologues were taken as that of (5) with the addition of the Fermi contact, dipolar and electric quadrupole terms for ^{135}Ba and ^{137}Ba:

$$b_F(^{135,137}\text{Ba})\mathbf{I}\cdot\mathbf{S} + c(^{135,137}\text{Ba})\left(I_zS_z - \frac{1}{3}\mathbf{I}\cdot\mathbf{S}\right) + eq_0Q(^{135,137}\text{Ba})\frac{3I_z - \mathbf{I}^2}{4I(2I-1)}. \quad (6)$$

The field-free eigenvalues and eigenvectors for the $X\,^2\Sigma^+$ $(v=0)$ state were obtained by numerical diagonalization of the representation constructed in a sequentially coupled Hund's case $(a_{\beta J})$ basis set. The representation for ^{138}BaF was of dimension 4 $[=(2S+1)\times[2I(^{19}\text{F})+1]]$, whereas the representation for the odd isotopologues was 16 $[=(2S+1)\times[2I(^{19}\text{F})+1]\times[2I(^{135,137}\text{Ba})+1]]$. The expressions for the matrix elements were taken from Ref. [31].

Combination difference revealed that the $A\,^2\Pi_{3/2}$ $(v=0)$ substate levels of the ^{135}BaF and^{137}BaF isotopologues exhibited no magnetic hyperfine splitting. Furthermore, no Λ doubling in the $A\,^2\Pi_{3/2}$ $(v=0)$ substate was observed.

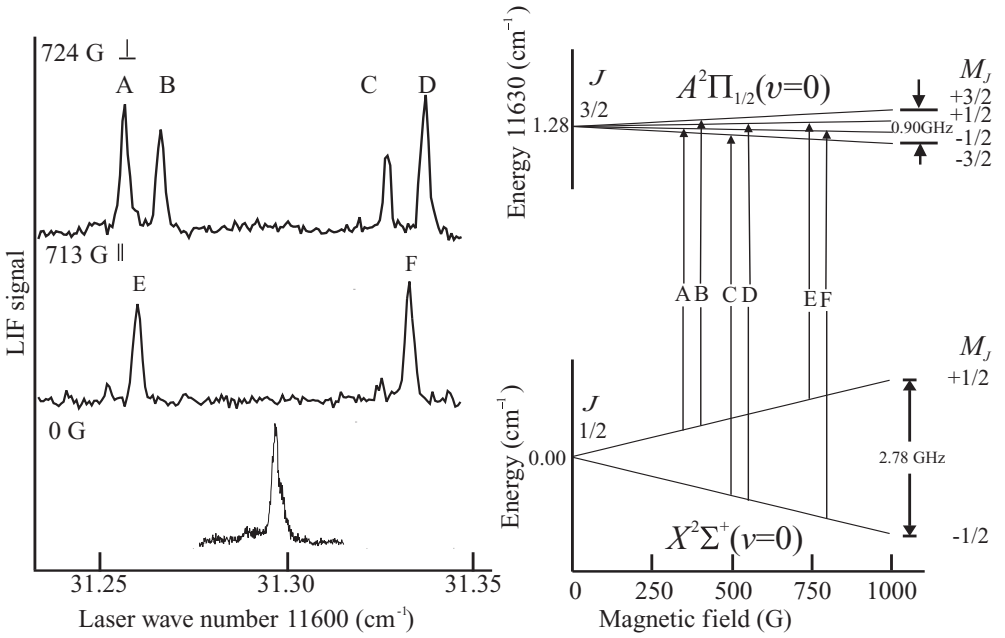

FIG. 10. $R_1(0)$ line of the ^{138}BaF isotopologue recorded field free (bottom) and in the presence of a 713 G parallel (middle) and a 724 G perpendicular (top) magnetic field. The associated energy levels as a function of applied magnetic field, and the assigned transitions, are also presented.

The Λ doubling in the Hund's case (*a*) limit $^2\Pi_{3/2}$ and $^2\Pi_{1/2}$ substate goes approximately as qJ^2 and $(p+2q)J$ [31], respectively. Therefore, the energies for the $A\,^2\Pi$ $(v=0)$ state were modeled by including the origin ($T_{0,0}$), spin-orbit interaction (A) and the associated centrifugal distortion correction (A_D), rotation (B) and the associated centrifugal distortion correction (D), the Λ doubling ($p+2q$), which affects the $A\,^2\Pi_{1/2}$ $(v=0)$ subband, and the Λ-type magnetic hyperfine $d(^{135,137}\mathrm{Ba})$ interaction terms:

$$\mathbf{H}^{\mathrm{eff}}(^2\Pi) = T_{0,0} + AL_zS_z + \tfrac{1}{2}A_D[L_zS_z,\mathbf{R}]^+ + B\mathbf{R}^2 - D(\mathbf{R}^2)^2 + \tfrac{1}{2}(p+2q)(e^{-2i\phi}J_+S_+ + e^{+2i\phi}J_-S_-) + \tfrac{1}{2}d(e^{-2i\phi}I_+S_+ + e^{+2i\phi}I_-S_-). \quad (7)$$

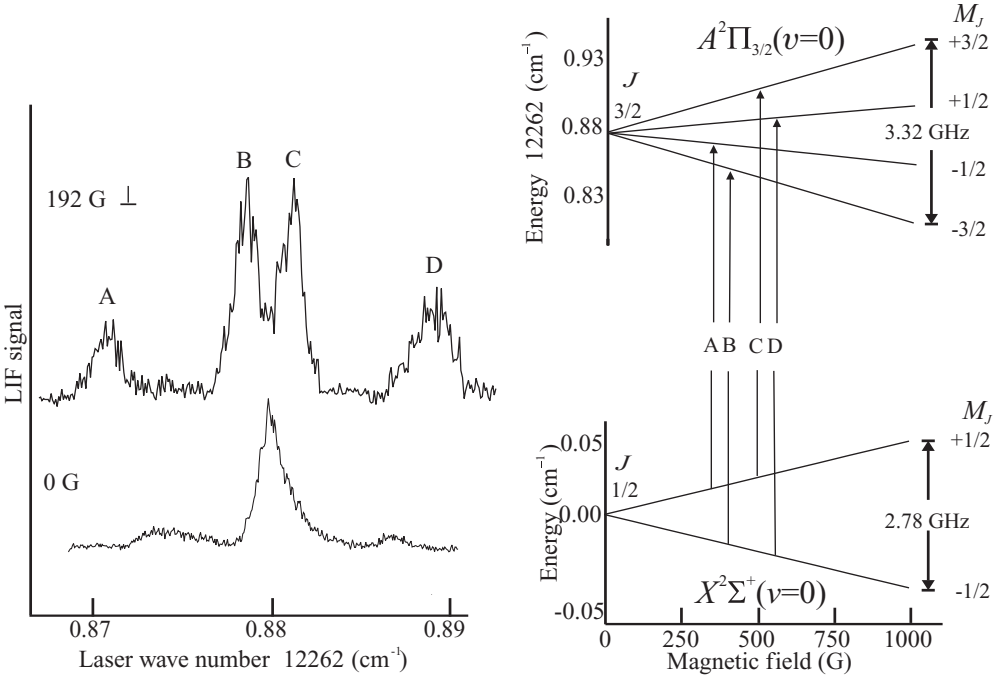

FIG. 11. $^SR_{21}(0)$ line of the ^{138}BaF isotopologue recorded field-free (bottom) and in the presence of a 192 G perpendicular (top) magnetic field. The associated energy levels as a function of applied magnetic field, and the assigned transitions, are also presented.

TABLE II. Observed and calculated Zeeman shifts for the $A\,^2\Pi$–$X\,^2\Sigma^+$(0,0) band system of ^{138}BaF.

Branch	Field (G)	M'_J	M''_J	Obs (MHz)	Dif (MHz)	Branch	Field (G)	M'_J	M''_J	Obs (MHz)	Dif (MHz)
$R_1(0)$, ∥	948	1/2	1/2	−1387	26	$R_1(0)$, ⊥	250	3/2	1/2	−402	21
	948	−1/2	−1/2	1408	−3		250	−1/2	1/2	−297	25
	931	1/2	1/2	−1442	−54		250	1/2	−1/2	331	10
	931	−1/2	−1/2	1419	33		250	−3/2	−1/2	423	0
	833	1/2	1/2	−1227	14	$^sR_{21}(0)$,∥	137	1/2	1/2	−111	4
	833	−1/2	−1/2	1243	3		137	−1/2	−1/2	128	15
	713	1/2	1/2	−1127	−65		141	1/2	1/2	−106	12
	713	−1/2	−1/2	1094	33		141	−1/2	−1/2	117	0
	482	1/2	1/2	−766	−48		192	1/2	1/2	−166	−4
	482	−1/2	−1/2	742	24		192	−1/2	−1/2	172	13
	248	1/2	1/2	−412	−43		228	1/2	1/2	−183	9
	248	−1/2	−1/2	387	18		228	−1/2	−1/2	192	4
	136	1/2	1/2	−249	−46		230	1/2	1/2	−206	−12
	136	−1/2	−1/2	211	8		230	−1/2	−1/2	175	−14
$R_1(0)$,⊥	948	3/2	1/2	−1578	28		253	1/2	1/2	−207	7
	948	−1/2	1/2	−1176	44		253	−1/2	−1/2	230	21
	948	1/2	−1/2	1211	−7		254	1/2	1/2	−226	−12
	948	−3/2	−1/2	1612	9		254	−1/2	−1/2	193	−16
	833	3/2	1/2	−1372	39		307	1/2	1/2	−244	16
	833	−1/2	1/2	−1035	37		307	−1/2	−1/2	271	19
	833	1/2	−1/2	1060	−11		310	1/2	1/2	−279	−17
	833	−3/2	−1/2	1417	8		310	−1/2	−1/2	242	−13
	724	3/2	1/2	−1214	−18	$^sR_{21}(0)$,⊥	141	−1/2	1/2	−265	10
	724	−1/2	1/2	−984	−52		141	1/2	−1/2	267	−6
	724	1/2	−1/2	912	19		192	−1/2	1/2	−374	1
	724	−3/2	−1/2	1207	−18		192	3/2	1/2	51	−1
	604	3/2	1/2	−1017	6		192	−3/2	−1/2	−49	5
	604	−1/2	1/2	−759	18		192	1/2	−1/2	383	11
	604	1/2	−1/2	774	−2		228	−1/2	1/2	−459	−13
	604	−3/2	−1/2	1009	−13		228	1/2	−1/2	445	4
	489	3/2	1/2	−816	12		230	−1/2	1/2	−459	−11
	489	−1/2	1/2	−612	17		230	3/2	1/2	48	−14
	489	1/2	−1/2	612	−17		230	−3/2	−1/2	−78	−14
	489	−3/2	−1/2	820	−7		254	−1/2	1/2	−517	−21
	364	3/2	1/2	−611	5		254	3/2	1/2	58	−10
	364	−1/2	1/2	−458	10		254	−3/2	−1/2	−85	−14
	364	1/2	−1/2	470	2		310	3/2	1/2	63	−20
	364	−3/2	−1/2	625	9		310	−3/2	−1/2	−107	−19

Standard deviation of fit = 21.5 MHz.

In Eq. (7) $J_\pm$, $S_\pm$, and $I_\pm$ are the shift operators of the total angular momentum in the absence of nuclear spin **J**, the total electron spin **S**, and the ^{135,137}Ba nuclear spin angular momentum $\mathbf{I_1}$, and ϕ is the azimuthal coordinate of the electrons. $[L_zS_z,\mathbf{R}]^+$ is the anticommutator. The field-free eigenvalues and eigenvectors for the $A\,^2\Pi$ ($v=0$) state were obtained by numerical diagonalization of the representation constructed in a sequentially coupled Hund's case ($a_{\beta J}$) basis set. The representation for ^{138}BaF was of dimension 8 $[=2\times(2S+1)\times[2I(^{19}\mathrm{F})+1]]$, whereas the representation for the odd isotopologues was 32 $[=2\times(2S+1)\times[2I(^{19}\mathrm{F})+1]\times[2I(^{135,137}\mathrm{Ba})+1]]$. The expressions for the matrix elements were taken from Ref. [31].

Various fits of the measured field-free spectrum were performed. The 267 measured field-free transitions [30] for the ^{138}BaF isotopologue were modeled by varying $T_{0,0}$, A, A_D, B, and $(p+2q)$. The centrifugal distortion correction to the rotational parameters, D, for the $A\,^2\Pi$ ($v=0$) state was held fixed to the value determined from the analysis of the high-temperature optical spectrum [15]. For the $X\,^2\Sigma^+$ ($v=0$) state, the B and γ parameters were constrained to the microwave values [10], the magnetic hyperfine parameters $b_F(^{19}\mathrm{F})$ and $c(^{19}\mathrm{F})$ were constrained to MODR values [12] and D to the high temperature optical spectrum [15]. The optimized parameters and associated errors are given in Table III. The standard deviation of the fit ($=0.0013$ cm^{-1}) is commensurate with the estimated measurement error.

Least-squares fitting of the 99 measured lines for the ^{137}BaF isotopologue [30] proceeded in a similar fashion. The fine and magnetic hyperfine parameters of the $X\,^2\Sigma^+$ ($v=0$) state were constrained to values extracted from the analysis of the pure rotational spectrum [11] with the exception of D which was constrained to the value obtained from the analysis of the ^{138}BaF optical spectrum [15] scaled by the expected mass ratio;

TABLE III. Field-free spectroscopic parameters in wave numbers (cm^{-1}) for the $A\,^2\Pi$–$X\,^2\Sigma^+$ (0,0) band system of BaF.

Parameter	^{138}BaF	^{137}BaF	^{135}BaF
$X\,^2\Sigma^+(v=0)$			
B	0.21594802[a]	0.21613878[b]	0.21675(5)
$10^7\times D$	1.85[c]	1.85[c]	1.85[d]
γ	0.00269930[a]	0.002702703[b]	0.00270270[d]
b_F(Ba)	NA	0.077587[b]	0.0702(5)
c(Ba)	NA	0.0250173[b]	0.002237381[e]
eq_0Q(Ba)	NA	−.00390270[b]	−0.003490348[e]
b_F(F)	0.002209862[f]	0.002209873[b]	0.002209873[b]
c(F)	0.000274323[f]	0.000274323[b]	0.000274323[b]
$A\,^2\Pi$ $(v=0)$			
A	632.28175(6)	632.2802(8)	632.2803(10)
$10^5\times A_D$	3.1(2)	3.1[d]	3.1[d]
B	0.2117414(10)	2.11937(12)	0.2125(4)
$10^7\times D$	2.00[c]	2.00[c]	2.00[c]
$(p+2q)$	−0.25755(10)	−0.2581(2)	−0.25755[c]
d(Ba)	NA	0.0076(10)	0.00685[e]
T_00	11946.3168(2)	11945.3152(6)	11946.3034(10)
Std. Dev.	0.0013	0.0014	0.0015

[a]Reference [10].
[b]Reference [11].
[c]Reference [15].
[d]Constrained to value scaled from the fit of the ^{138}BaF transitions.
[e]Constrained to value obtained from scaling the value for ^{137}BaF.
[f][f] Ref. [12].

i.e., scaled by $[\mu(^{138}\text{BaF})]^2/[\mu(^{137}\text{BaF})]^2$ where μ = reduced mass. Five parameters for the $A\,^2\Pi$ $(v=0)$ state were varied: A, B, $(p+2q)$, $d(^{137}\text{Ba})$, and T_{00}. A_D was constrained to the value extracted from the analysis of the ^{138}BaF measurements [11] and D to the value obtained from isotopically scaling the ^{138}BaF value. The optimized parameters and associated errors are given in Table III. The standard deviation of the fit ($=0.0014$ cm^{-1}) is commensurate with the estimated measurement error.

There are no previously determined parameters for the ^{135}BaF isotopologue. Fitting of the 73 measured and assigned transitions [30] was performed by varying a subset of both the $X\,^2\Sigma^+$ $(v=0)$ and $A\,^2\Pi$ $(v=0)$ state parameters. In the $X\,^2\Sigma^+$ $(v=0)$ state, only B and b_F (Ba) were varied. The parameter D was constrained to the ^{138}BaF scaled by the known mass dependence and the $c(^{135}\text{Ba})$ and $eq_0Q(^{135}\text{Ba})$ parameters to those for ^{137}Ba scaled by the nuclear g factors and quadrupole moment, respectively. The fluorine magnetic hyperfine parameters for ^{137}BaF, $b_F(^{19}\text{F})$ and $c(^{19}\text{F})$, were constrained to the ^{138}BaF values [10]. The origin T_{00}, rotational constant B, and spin-orbit parameter A for the $A\,^2\Pi$ $(v=0)$ state of the ^{137}BaF isotopologue were varied. The parameters A_D and $(p+2q)$ were constrained to the ^{138}BaF values, D to the mass scaled ^{138}BaF value, and d(Ba) to the ^{137}BaF value scaled by the nuclear g factors. The standard deviation of the fit ($=0.0015$ cm^{-1}) is commensurate with the estimated measurement error.

TABLE IV. Optimized magnetic g factors $A\,^2\Pi(v=0)$ and $X\,^2\Sigma^+(v=0)$ states of ^{138}BaF.

Parameter[a]	Value	Correlation matrix		
$g_l'(A\,^2\Pi)$	−0.536(23)	1		
$g_L'(A\,^2\Pi)$	0.980(35)	−0.6497	1	
$g_l(X\,^2\Sigma^+)$	−0.028(13)	0.2233	0.2314	1

[a]g_s for the $A\,^2\Pi(v=0)$ and $X\,^2\Sigma^+(v=0)$ states constrained to 2.002, $g_l(A\,^2\Pi)$ was set to zero.

TABLE V. Permanent electric dipole moments (debye, D) for the alkaline-earth-metal monofluorides.

	CaF		SrF		BaF	
State	Value	Ref.	Value	Ref.	Value	Ref.
$X\,^2\Sigma^+$	3.07(7)	[33]	3.4963(6)	[35]	3.170(3)	[12]
$A\,^2\Pi_{1/2}$	–	–	–		1.50(2)	Present
$A\,^2\Pi_{3/2}$	2.45(6)	[34]	2.06(5)	[36]	1.31(2)	Present

B. Stark effect and intensities

The interaction between the static electric field $\mathbf{E}$ and the molecular electric dipole moment operator μ is represented by the Stark Hamiltonian:

$$\mathbf{H}^{\text{Stark}} = -\boldsymbol{\mu}\cdot\mathbf{E}. \tag{8}$$

The matrix representation of $\mathbf{H}^{\text{Stark}}$ is block diagonal in M_F but of infinite dimension. The predicted Stark shifts in the $X\,^2\Sigma^+(v=0)$ state of the ^{138}BaF isotopologue were obtained by numerical diagonalization of a 16×16 truncated matrix representation constructed using the Hund's case $(a_{\beta J})$ basis functions for $F=0$–4. The observed Stark shifts of Table I were used as input into a nonlinear least-squares fitting program in which μ_e for the $X\,^2\Sigma^+(v=0)$ was held fixed to the previously determined value [$=3.170(3)$ D] [12] and μ_e for the $A\,^2\Pi$ $(v=0)$ state was optimized. Initial attempts to simultaneously fit the shifts of the $^SR_{21}(0)$ and $^OP_{12}(2)$ lines revealed systematic deviations indicating that the μ_e values for the $A\,^2\Pi_{1/2}$ and $A\,^2\Pi_{3/2}$ spin-orbit states are significantly different. Independent fits of the Stark shifts of the $^SR_{21}(0)$ and $^OP_{12}(2)$ lines determined μ_e of 1.50(2) and 1.31(2) D for the $A\,^2\Pi_{1/2}(v=0)$ and $A\,^2\Pi_{3/2}$ $(v=0)$ states, respectively. The error estimates represent a 90% confidence limit. The standard deviation of the fits for the $^SR_{21}(0)$ and $^OP_{12}(2)$ lines were 8 and 5 MHz, respectively, which are commensurate with the measurement uncertainty.

Modeling the spectra greatly assisted in the assignment of quantum numbers, particularly in the case of the overlapped spectra for the ^{135}BaF and ^{137}BaF isotopologues. Spectra for the ^{138}BaF isotopologue were modeled by constructing a 4×8 Hund's case $(a_{\beta J})$ electric dipole transition moment matrix and cross multiplying the transition matrix by the $X\,^2\Sigma^+$ and $A\,^2\Pi$ $(v=0)$ eigenvectors. The transition moment was squared and multiplied by a Boltzmann factor, and a Lorentzian line shape was superimposed on each spectral feature and co-added. Spectra for the ^{135}BaF and ^{137}BaF isotopologues were modeled in a similar fashion, but with the 16×32 Hund's case $(a_{\beta J})$ electric dipole transition moment matrix.

C. Zeeman effect

The effective Zeeman Hamiltonian was taken as [31,32]:

$$\hat{H}^{\mathrm{Zee}}(\mathrm{eff}) = g_S\mu_B\hat{\mathbf{S}}\cdot\hat{\mathbf{B}} + g_l'\mu_B\hat{\mathbf{L}}\cdot\hat{\mathbf{B}} + g_l\mu_B(\hat{S}_x\hat{B}_x + \hat{S}_y\hat{B}_y) + g_l'\mu_B(e^{-2i\varphi}\hat{S}_+\hat{B}_+ + e^{+2i\varphi}\hat{S}_-\hat{B}_-). \quad (9)$$

The rotational g factors, g_r and g_r', were not included because their effects are expected to be negligibly small for the low rotational levels investigated. In the effective Hamiltonian model, both g_S and g_L' are treated as adjustable parameters to account for electronic state mixing [31].

The matrix representation of $\hat{\mathbf{H}}^{\mathrm{Zee}}$(eff) is of infinite order. The very small ^{19}F magnetic hyperfine splitting was not resolved in the Zeeman spectra (see Figs. 10 and 11) due to inhomogeneous and residual fields, and the energy levels can be characterized by the projection quantum number M_J. Eigenvalues and eigenvectors for the lowest rotational levels of the $A\,^2\Pi(v=0)$ and $X\,^2\Sigma^+(v=0)$ states investigated here were obtained by numerical diagonalization of an 8×8 and 16×16 matrix representations, respectively, constructed from the $J=0.5$ to $J=3.5$ Hund's case (a) basis functions. The expressions for the matrix elements were taken from Ref. [31]. The 76 magnetically induced Zeeman shifts of Table II, and initial estimates of the g factors for the $A\,^2\Pi(v=0)$ and $X\,^2\Sigma^+$ $(v=0)$ states, were input for a nonlinear least-squares fitting process. Initial attempts to simultaneously optimize g_S, g_L', g_l, and g_l' for the $A\,^2\Pi$ state and g_l and g_S for $X\,^2\Sigma^+$ produced a highly correlated set of parameters. In the end, the g_S parameter for the $A\,^2\Pi$ $(v=0)$ and $X\,^2\Sigma^+$ $(v=0)$ states was held fixed at 2.002 because the nonadiabatic contributions to this parameter are expected to be small [31]. In addition, $g_l(A\,^2\Pi)$, which is predicted to be small (*vide infra*) was set to zero. The optimized values for g_l $[X\,^2\Sigma^+(v=0)]$, $g_l'[A\,^2\Pi(v=0)]$, and g_L' $[A\,^2\Pi(v=0)]$, along with their associated errors and correlation matrix, are listed in Table V. The standard deviation of the fit was 34 MHz, which is commensurate with the estimated measurement accuracy.

V. DISCUSSION

A primary objective of the current study was to determine a set of spectroscopic parameters that could be used to predict the eigenvalues and eigenvectors for the $A\,^2\Pi(v=0)$ and $X\,^2\Sigma^+(v=0)$ states of the three major isotopologues of barium monofluorides, both field-free and in the presence of static magnetic and electric fields. As can be seen from the comparison of the predicted and observed spectra given in Figs. 3–6, 8, and 9, the determined spectroscopic constants accurately reproduce the energies and eigenvectors at fields appropriate for future PNC measurements. The observed ^{135}Ba and ^{137}Ba hyperfine structure in the low rotational levels of the $A\,^2\Pi_{1/2}(v=0)$ substate can be modeled using solely the d(Ba) magnetic hyperfine parameter. The $A\,^2\Pi_{3/2}(v=0)$ substate exhibited no hyperfine structures.

Surprisingly, the semiempirical electrostatic model predictions by Törring *et al.* [19] and Mestdagh and Visticot [20] which predict μ_e values of approximately 5 D for the $A\,^2\Pi$ are in very poor agreement with observation. The LFT prediction [21] of 3.45 D for the $A\,^2\Pi$ states is only slightly better. The determined μ_e values for BaF are compared with values for isovalent CaF [33,34] and SrF [35,36] in Table V. Only the μ_e values for the $A\,^2\Pi_{3/2}$ $(v=0)$ spin-orbit state were measured for CaF and SrF. For all three molecules there is an observed large decrease in μ_e upon excitation from the $X\,^2\Sigma^+$ state to the $A\,^2\Pi$ state. This is qualitatively explained as the result of promoting the sole unpaired electron from a metal-ion-centered ns orbital ($n=4$, 5, and 6 for Ca, Sr, and Ba) to a more highly polarizable $np_{\pm1}/(n-1)d_{\pm1}$ hybrid orbital. The effect becomes more pronounced down the series with the ratios $\mu_e(A\,^2\Pi_{3/2})/\mu_e(X\,^2\Sigma^+)$ being 0.79, 0.59, and 0.41 for CaF, SrF, and BaF, respectively. This mimics the trend in static average electric dipole polarizabilities for the ground states of Ca ($=23$ Å^3), Sr ($=28$ Å^3), and Ba ($=56$ Å^3).

The observation that $\mu_e(A\,^2\Pi_{1/2})$ $[=1.50(2)$ D] is larger than $\mu_e(A\,^2\Pi_{3/2})$ $[=1.31(2)$ D] must result from a complicated spin-orbit mixing of the $A\,^2\Pi$ state with the nearby $A'^2\Delta$ ($T_e\approx$ 10940 cm^{-1}), $B\,^2\Sigma^+$ ($T_e\approx$ 14040 cm^{-1}), and $C\,^2\Pi$ ($T_e\approx$ 20091 cm^{-1}) states. LFT [20], which does not account for spin-orbit mixing, predicts that $\mu_e(A'^2\Delta)$ and $\mu_e(C\,^2\Pi)$ are greater than $\mu_e(A\,^2\Pi)$ which in turn is comparable to $\mu_e(B\,^2\Sigma^+)$. According to LFT, $\mu_e(A'^2\Delta)$ is large because, to a first approximation, the sole unpaired electron is in a compact Ba$^+$-centered $5d$ orbital and $\mu_e(C\,^2\Pi)$ is large because the sole unpaired electron is in a Ba$^+$-centered $5d$-$6p$ hybrid orbital that is pointed toward the F nucleus. Furthermore, according to LFT, $\mu_e(A\,^2\Pi)\approx\mu_e(B\,^2\Sigma^+)$ because the LFT predicted $5d$ and $6p$ composition for the two states is approximately identical. Evidently the $A\,^2\Pi_{1/2}$ state is more strongly mixed with the $C^2\Pi$ and $A'^2\Delta$ states than is the $A\,^2\Pi_{3/2}$ state. A similar effect has been observed in CaOH and SrOH [36].

The determined Zeeman parameters can also be qualitatively understood. An estimate for g_l $(X\,^2\Sigma^+)$ is obtainable from the Curl relationship [32]:

$$g_l \approx -\gamma/2B, \quad (10)$$

where γ and B, are the spin-rotation and rotational parameters. Using the parameters from Table III, (10) gives $g_l(X\,^2\Sigma^+)=0.00625$ which is the correct sign but about a factor of 4 too small. The parity-dependent anisotropic g factor for the $A\,^2\Pi$ state can be approximated using an equation analogous to the Curl relationship [31]:

$$g_l' \approx p/2B, \quad (11)$$

where p is the Λ-doubling parameter. It is reasonable to assume that $q=0$, and thus that $p=0.2575$ cm^{-1}, since no Λ doubling in the $A\,^2\Pi_{3/2}$ levels was observed. (11) predicts that $g_l'\approx 0.2575/(2\times 0.21954)=0.5866$, which is in very good agreement with the experimental value $[=0.536(23)]$. In fitting the Zeeman shifts, g_l for the $A\,^2\Pi$ was constrained to zero. It is difficult to estimate g_l for the $A\,^2\Pi$ from the Curl relationship [Eq. (10)] because the required spin-rotation parameter γ for the $A\,^2\Pi$ state is not determined. Brown and Watson [36] have shown that for a $^2\Pi$ state, γ and A_D, the centrifugal distortion correction to the spin-orbit coupling, are totally correlated. When γ is constrained to zero, as was done

here, then the fitting parameter A_D is a linear combination of the true values for A_D and γ [37]:

$$A_D^{\text{fitting}} \approx A_D^{\text{true}} - \gamma \frac{2B}{(A-2B)}. \quad (12)$$

An upper limit for γ ($A\,^2\Pi$) of 0.046 cm^{-1} is obtained from Eq. (12) by assuming that $A_D^{\text{true}} = 0$. The Curl relationship then predicts an approximate value for $g_l(A\,^2\Pi)$ of $+0.11$.

VI. CONCLUSION

A cold molecular beam sample of BaF has been generated by laser vaporization techniques and the $A\,^2\Pi$–$X\,^2\Sigma^+$ (0,0) band system recorded at near the natural linewidth limit both field-free and in the presence of static magnetic and electric fields. A set of effective spectroscopic parameters has been generated that can reproduce the energies at field strengths appropriate for proposed PNC measurements. The determined hyperfine parameters, magnetic g factors, and permanent electric dipole moments are benchmarks for evaluation of future predictions of the excited $A\,^2\Pi$ state.

ACKNOWLEDGMENTS

This research has been supported by the National Science Foundation, Experimental Physical Chemistry (Grant 943360412) and Physics (Grant PHY-0758045). The authors thank Dr. Jinhai Chen for assistance in the measurements.

[1] M. G. Kozlov, A. V. Titov, N. S. Mosyagin, and P. V. Souchko, Phys. Rev. A **56**, R3326 (1997)
[2] A. V. Titov, N. S. Mosyagin, A. N. Petrov, and T. A. Isaev, Int. J. Quantum Chem. **104**, 223 (2005)
[3] M. K. Nayak, and R. K. Chaudhuri, J. Phys. B **39**, 1231 (2006).
[4] A. V. Titov, N. S. Mosyagin, A. N. Petrov, T. A. Isaev, and D. P. DeMille, Prog. Theor. Chem. Phys. **15**, 253 (2006).
[5] M. K. Nayak, R.K. Chaudhuri, and B. P. Das, Phys. Rev. A **75**, 022510 (2007).
[6] M. K. Nayak and R. K. Chaudhuri, Phys. Rev. A **78**, 012506 (2008).
[7] M. K. Nayak and B. P. Das, Phys. Rev. A **79**, 060502 (2009).
[8] D. DeMille, S. B. Cahn, D. Murphree, D. A. Rahmlow, and M. G. Kozlov, Phys. Rev. Lett. **100**, 023003(2008)
[9] M. G. Kozlov and L. N. Labzowsky, J. Physics B **28**, 1933 (1995).
[10] Ch. Rayzlewicz and T. Törring, Chem. Phys. **51**, 329 (1980).
[11] Ch. Rayzlewicz, H.-U. Schütze-Pahlmann, J. Hoeft, and T. Törring, Chem. Phys. **71**, 389 (1982).
[12] W.E. Ernst, J. Kändler, and T. Törring, J. Chem. Phys. **84**, 4769 (1986).
[13] B. Guo, K. Q. Zhang, and P.F. Bernath, J. Mol. Spectrosc. **170**, 59, (1995).
[14] C. Effantin, A. Bernard, J. D'Incan, G. Wannous, J. Verges, and R. F. Barrow, Mol. Phys. **70**, 735 (1990).
[15] A. Bernard, C. Effantin, J. D'Incan, J. Verges, and R. F. Barrow, Mol. Phys. **70**, 747 (1990).
[16] A. Bernard, C. Effantin, E. Andrianavalona, J. Verges, and R. F. Barrow, J. Mol. Spectrosc. **152**, 174 (1992).
[17] L.-E. Berg, N. Gador, D. Husain, H. Ludwigs, and P. Royen, Chem. Phys. Lett. **287**, 89 (1998).
[18] L.-E. Berg, T. Olsson, J. C. Chanteloup, A. Hishikawa, and P. Royen, Mol. Phys. **79**, 721 (1993).
[19] T. Törring, W.E. Ernst, and J. Kändler, J. Chem. Phys. **90**, 4927 (1989).
[20] J. M. Mestdagh and J.P. Visticot, Chem. Phys. **155**, 79 (1991).
[21] A. R. Allouche, G. Wannous, and M. Aubert-Frécon, Chem. Phys. **170**, 11 (1993).
[22] A.T. Le, H. Wang, and T.C. Steimle, Phys. Rev. A **80**, 062513 (2009).
[23] T. C. Steimle, T. Ma, and C. Linton, J. Chem. Phys. **127**, 234316 (2007).
[24] T. Ma, C. Butler, J. M. Brown, C. Linton, and T. C. Steimle, J. Phys. Chem. A. **113**, 8038 (2009).
[25] S. Gerstenkorn and P. Luc, *Atlas du Spectre d'Absorption de la Molecule de l'Iode* (CNRS, Paris, 1978); S. Gerstenkorn and P. Luc, Rev. Phys. Appl. **14**, 791 (1979).
[26] S. Gerstenkorn, P. Luc, and R. Vetter, Rev. Phys. Appl. **16** 529 (1981).
[27] T. C. Steimle, J. Gengler, and J. Chen, Can. J. Chem. **82**, 779 (2004).
[28] T. C. Steimle, Int. Rev. Phys. Chem. **19**, 455 (2000).
[29] G. Herzberg, *Molecular Spectra and Molecular Structure* (Van Nostrand Reinhold, New York, 1950).
[30] See Supplemental Material at http://link.aps.org/supplemental/10.1103/PhysRevA.84.012508 for tables.
[31] J. M. Brown and A. Carrington, *Rotational Spectroscopy of Diatomic Molecules* (Cambridge University, Cambridge, England, 2003).
[32] W. Weltner Jr., *Magnetic Atoms and Molecules* (Dover, New York, 1983).
[33] W. J. Childs, L. S. Goodman, U. Nielsen, and V. J. Pfeufer, Chem. Phys. **80**, 2283 (1984).
[34] W. E. Ernst and J. Kaendler, Phys. Rev. A: Atomic, Molecular, and Optical Physics **39**, 1575 (1989).
[35] W. E. Ernst, J. Kaendler, S. Kindt, and T. Toerring, Chem. Phys. Lett. **113**, 351 (1985).
[36] J. Kaendler, T. Martell, and W. E. Ernst, Chem. Phys. Lett. **155**, 470 (1989).
[37] T. C. Steimle, D. A. Fletcher, K.Y. Jung, and C.T. Scurlock, J. Chem. Phys. **96**, 2556 (1992).
[38] J. M. Brown and J .K. G. Watson, J. Mol. Spectrosc. **65**, 65 (1977).